A Letters Journal Exploring the Frontiers of Physics

October 2014

EPL, **108** (2014) 24001
doi: 10.1209/0295-5075/108/24001

www.epljournal.org

Drops can bounce from perfectly hydrophilic surfaces

J. M. Kolinski[1,2], L. Mahadevan[1,3] and S. M. Rubinstein[1,2]

[1] *School of Engineering and Applied Sciences, Harvard University - Cambridge, MA 02138, USA*
[2] *Department of Physics of Complex Systems, Weizmann Institute of Science - Rehovot 76100, Israel*
[3] *Department of Physics, Harvard University - Cambridge, MA 02138, USA*

received 14 August 2014; accepted in final form 23 September 2014
published online 9 October 2014

PACS 47.55.D- – Drops and bubbles
PACS 47.55.N- – Interfacial flows
PACS 68.03.-g – Gas-liquid and vacuum-liquid interfaces

Abstract – Drops are well known to rebound from superhydrophobic surfaces and from liquid surfaces. Here, we show that drops can also rebound from a superhydrophilic solid surface such as an atomically smooth mica sheet. However, the coefficient of restitution C_R associated with this process is significantly lower than that associated with rebound from superhydrophobic surfaces. A direct imaging method allows us to characterize the dynamics of the deformation of the drop in entering the vicinity of the surface. We find that drop bouncing occurs without the drop ever touching the solid and there is a nanometer-scale film of air that separates the liquid and solid, suggesting that shear in the air film is the dominant source of dissipation during rebound. Furthermore, we see that any discrete nanometer-height defects on an otherwise hydrophilic surface, such as treated glass, completely inhibits the bouncing of the drop, causing the liquid to wet the surface. Our study adds a new facet to the dynamics of droplet impact by emphasizing that the thin film of air can play a role not just in the context of splashing but also bouncing, while highlighting the role of rare surface defects in inhibiting this response.

The impact of liquid droplets on solid surfaces is ubiquitous in many natural and industrial settings. Depending on the impact parameters, a liquid drop may spread, break up, splash or bounce [1]. While spreading and splashing occur under a wide range of conditions [1–5], it is traditionally thought that drops will only bounce from solid surfaces that are special: heated beyond the boiling temperature of the impacting liquid [6] or superhydrophobic; textured and functionalized to comply with a Cassie-Baxter state, wherein the liquid is supported by micron-sized asperities and the interstitial air [7–10]; additionally, drops are well known to rebound from liquid surfaces [11]. Here we show that this is not the case: drops can bounce from any smooth enough hydrophilic surface at room temperature as well. Indeed, drops were observed to rebound from glass, silicon wafers and from mica; thus, drop rebound appears to be a general phenomenon for impact upon smooth, defect free surfaces.

Our experiments were carried out by impacting drops upon a freshly cleaved mica surface, which is a hydrophilic surface with a vanishing contact angle, as shown in fig. 1(b). We find that if the impact velocity V is below a critical value, $V_c = 0.75\,\mathrm{m/s}$, then the drop will rebound, while above V_c, the drop will wet the surface. Similar rebound events are observed for impacting drops of silicon oil as well as for impact on clean glass slides. This suggests that when the drop bounces it never contacts the substrate, and instead is cushioned by a thin film of air [12]. Indeed, for $V < 0.2\,\mathrm{m/s}$, the drop does not visibly detach from the surface and bounce; instead, the drop oscillates above a steady thin film of air without fully retracting away from the solid surface. Similarly, for impact upon a superhydrophobic substrate at low V, the drop oscillates while in partial contact with the substrate [13]. The role of air in droplet impact has recently been the focus of much study and debate [2,5,12,14–23]. To understand the role played by air during the early dynamics of droplet impact, we use Total Internal Reflection (TIR) microscopy to directly observe the impact surface [12], as shown schematically in fig. 1(a). When the droplet enters the evanescent field above the impact surface, partially transmitted light results in a gray-scale image, as shown in fig. 1(c), which can be converted to a height profile h, as shown in fig. 1(d).

While TIR can resolve nanometer scales, its range is limited and cannot resolve the dynamics occurring more than

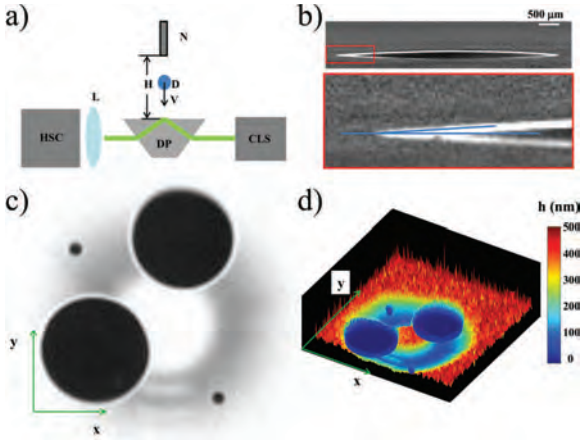

Fig. 1: (Color online) The experimental system. (a) A schematic of the experimental set-up. Drops (D) of 10 cSt water-glycerol solution, with a radius of 800 μm fall from a nozzle (N), from a height (H) above the substrate, whereupon the drop impacts with a velocity $V = (2gH)^{1/2}$. We illuminate the surface of a dove (DP) prism from below with a monochromatic, collimated light source (CLS) at an angle of incidence greater than the critical angle for total internal reflection for a glass-air interface, thus exciting an evanescent wave above the surface of the prism with a characteristic decay length, $\delta \sim \mathcal{O}(130\,\text{nm})$. The prism is optically coupled to the impact surface with immersion oil (Zeiss 518f). We use a long working distance objective (L) to image the beam as it exits the prism on the high-speed imaging sensor of our Phantom v711 fast camera (HSC) at frame rates exceeding 150 kHz. (b) The liquid drop totally wets the freshly cleaved, hydrophilic mica surface. (c) A typical snapshot from a drop impact event, the gray ring indicates the presence of a nanometer thin film of air above the surface and the four black circles are locations where the solid liquid contact occurred. (d) the same as (c); however, here gray-scale image intensity, $I(x, y, t)$ is normalized and converted to height as $h = -\delta \log(1 - \frac{I(x,y,t)}{I(x,y,0)})$ [12] and presented as a surface plot. Color indicates height in nanometers above the mica surface.

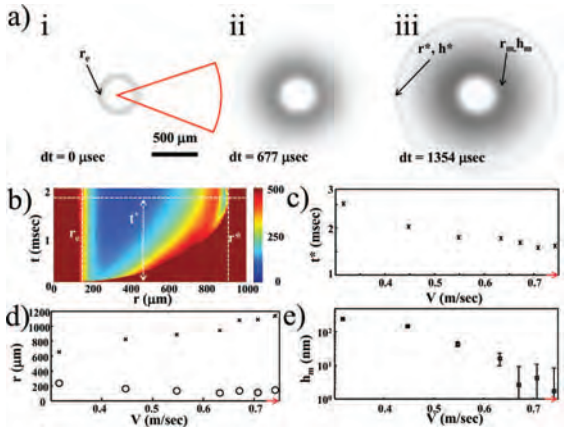

Fig. 2: (Color online) Impact dynamics of the drop. (a) Three consecutive TIR images corresponding to a drop impacting on a mica substrate with $H = 15\,\text{mm}$ ($V = 0.55\,\text{m/s}$). The red wedge is an annular region over which the height profiles are averaged, converted from gray-scale to height and then shown as an r-t plot in (b). Here, $dt = 0$ corresponds to the first frame where the liquid has entered within $h = 500\,\text{nm}$ of the surface. (b) An r-t plot for the entire impact event shown in (a), where color represents height from 0 to 500 nm. t^* indicates the total liquid spreading time; r^* and r_e are the greatest radial extent of the spreading liquid and the radial edge of the dimple, respectively. (c) t^* as a function of V. (d) r^* and r_e are shown as a function of V. (e) The height of the film at closest approach h_m, indicated in (a)iii., as a function of V. The critical velocity for rebound V_c is indicated by the red arrows along the horizontal axis in (c)–(e).

500 nm above the surface. As a result, the liquid enters the evanescent field after a dimple of compressed air between the drop and substrate has already formed [21], and appears as a ring, as shown in the fast-camera snapshot in fig. 2(a).i. As more fluid moves outward, it skates over the thin film of air, increasing the film's lateral dimension, as shown in fig. 2(a).ii. Ultimately, the liquid front arrests, the drop stops expanding as it reaches its greatest lateral extent, r^*, as shown in fig. 2(a).iii, and then starts to retract.

These dynamics are typical to all bouncing drops and can be represented in a single r-t plot, as shown in fig. 2(b). The radial location of the outward spreading liquid initially grows in time as $t^{1/2}$ [24], but eventually the liquid decelerates and halts at time $t^* \sim 1.8\,\text{ms}$, and radius $r^* \sim 900\,\mu\text{m}$, as indicated in fig. 2(b) by the dashed lines. Importantly, the liquid continues to slowly approach the surface as the air drains, as shown in fig. 2(b). t^* decreases with increasing V, as shown in fig. 2(c); nevertheless, r^* increases with V, as shown in fig. 2(d). As shown in fig. 2(e), as V increases, the height of the film at closest approach h_m decreases to a value where we expect the film to be unstable due to molecular forces [25]; thus, at the higher impact velocities, the rebound of the drop is enabled by the transient stabilization of the thin film of air.

To probe the dynamics of rebound, we compare images of identical rebounding drops from two experiments: one imaged from the side and the other with TIR, as shown in fig. 3(a) and in a supplementary video[1]. At $t^* = 1.8\,\text{ms}$, the droplet has spread to r^* and a dark gray ring appears at the rim; by this time the drop has deformed significantly from its originally spherical shape, as shown in fig. 3(a).ii. After spreading to r^*, the drop begins to retract from the surface; 3.6 ms after its initial approach to within nanometers of the surface, the radius of the film of air decreases to less than half of its greatest lateral extent, as shown in fig. 3(a).iii. Ultimately, after 5.7 ms have elapsed, the droplet completely exits the evanescent field, rebounding from the surface, as shown in fig. 3(a).iv. The liquid front spreads outward as $t^{1/2}$ but retracts at a nearly constant rate, $V_{rec} \sim 0.25\,\text{m/s}$, indicated by the line in fig. 3(b).

In spite of the asymmetry between the spreading and the retracting of the drop, the overall time it takes the drop

[1]Video accessible at `http://youtu.be/Nf810Ompreg`.

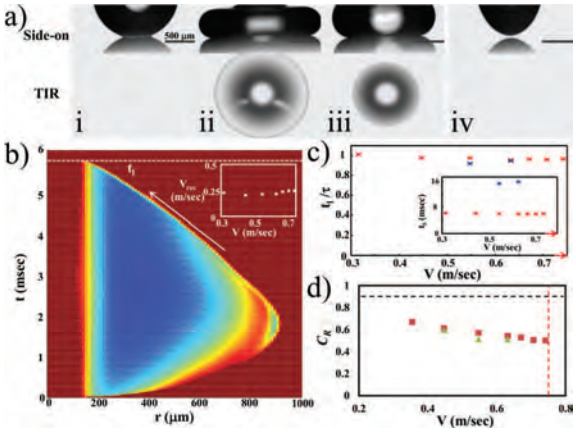

Fig. 3: (Color online) Drops bouncing off of mica surfaces. (a) A montage of fast-camera images taken from the side (top) and with TIR (bottom) of two identical experiments with $R = 800\,\mu$m and $H = 15\,$mm (video hosted online[2]). Frames i–iii are taken at an interval of 1.8 ms; frame iv is taken 6.5 ms after the first frame. (b) An r-t plot of the experiment shown in (a), color scale is as in fig. 2(b). The liquid retracts inwards at a nearly constant velocity V_{rec}, indicated by the white arrow. As a result of this asymmetry in the spreading and retraction rates, the outward spreading of the liquid lasts $\sim 1.8\,$ms, while its retraction persists for approximately double this time, as shown in the figure (inset). V_{rec} as a function of V. Note that $V_{rec} \sim 0.25\,$m/s remains practically unchanged for all impact velocities. The liquid entirely departs the evanescent field at $t = t_l$. (c) The drop residency time scaled by the drop oscillation period, t_l/τ as a function of V for two drop radii: $R = 0.8\,$mm (red "×") and $R = 1.6\,$mm (blue "×") (inset) t_l as a function of V. (d) The coefficient of restitution C_R as a function of V. V_c is indicated by the red arrows along the horizontal axis in (c), and the vertical dashed line in (d).

to complete a bouncing cycle, t_l, depends on drop radius R but not on V and is in agreement with the value for the period of an oscillating drop [26], $\tau = 2.2(\rho\frac{R^3}{\gamma})^{1/2}$, as shown in fig. 3(c), but inconsistent with the 18% difference reported for rebound from superhydrophobic surfaces [27]. Due to viscous losses not all the energy is conserved, so the bouncing drop does not rebound at its impact speed. We estimate the coefficient of restitution, C_R by measuring the original release height H_f and the maximal rebounding height H_r and calculate $\sqrt{\frac{H_r}{H_f}}$ as a proxy for the more commonly used definition of $C_R = V_r/V$. We find that C_R is independent of R, but decreases with V, as shown in fig. 3(d), never exceeding 0.65, much lower than the value of $C_R = 0.9$ for impact on superhydrophobic surfaces [7].

To understand this difference, we note that the deformation of the fluid drop induces large shear rates in the thin film of air and in the liquid drop itself. We estimate the viscous dissipation rate per unit length associated with the retracting liquid front with meridian radius of curvature r_e, which scales as $\mu_{liq}\,(\frac{U}{r_e})^2 r_e^2$, and the viscous dissipation rate associated with the shear in the air film, which scales as $\mu_{air}\left(\frac{U}{h}\right)^2 r_e h$. These contributions to the dissipation in the air film balance at a crossover thickness $h_{co} = \frac{\mu_{gas}}{\mu_{liq}} r_e$; in our experiment, with $\mu_{liq} = 10\,$cSt water-glycerol withdrawing from air and $r_e \sim \mathcal{O}(100\,\mu$m), which remains strikingly constant during the retraction phase, we expect dissipation to be dominant in the air for $h_{co} \lesssim \mathcal{O}(200\,$nm). This cross-over height is between the film thicknesses we observe above the mica surfaces, and the height of the pillars used to make superhydrophobic surfaces that exhibit reduced drag [28,29]. Counterintuitively, drops rebound from sparse contacts with superhydrophobic surfaces more vigorously [7] than from mica surfaces, where there is absolutely no contact, but a thinner film of air, as shown in the supplementary video[3].

During the retraction phase, the drop begins to lift off of the surface and air must enter the thin gap between the solid and liquid. Balancing the viscous power per unit length and liquid inertia per unit length with the driving power due to capillary forcing at the retracting front moving at velocity U yields $\mu_{air}\left(\frac{U}{h}\right)^2 hl + \rho U^2 Ul \sim \frac{\gamma}{r_e} Ul$. There are two limits that determine the retraction velocity. First, for large h, the viscous dissipation in the air can be neglected, and the front retracts at the classical Taylor-Culick velocity [13,30], $U \sim \sqrt{\frac{\gamma}{\rho r_e}} = \sqrt{\frac{0.7\,\mathrm{J/m^2}}{10^3\,\mathrm{kg/m^3}\cdot 10^{-4}\,\mathrm{m}}} = 0.84\,$m/s. The second limit arises for small h, when the viscous power dissipated in the air balances the driving power; in this limit, $U = \frac{h\gamma}{\mu_{air} r_e} \sim \frac{10\,\mathrm{nm}\ 0.7\,\mathrm{J/m^2}}{2\times 10^{-5}\,\mathrm{Pa{\cdot}s}\ 100\,\mu\mathrm{m}} \sim 0.35\,$m/s. For typical values of the experimental parameters, the retraction velocity calculated in the limit of small h is in qualitative agreement with the measured value of $U \sim 0.25\,$m/s, independent of the radial distance of the retracting front from the impact center (inset of fig. 3(c)).

The dynamics of rebound are truncated when the impact surface includes any asperities larger than the thickness of the film of air. Asperities that perforate the air layer nucleate a capillary bridge, causing the liquid to rapidly wick over the surface, thus binding the drop to the surface and preventing rebound. For a carefully cleaned glass surface, such asperities are rare, but occur with sufficient frequency to make drop rebound uncommon. A typical time series of asperity-nucleated contact is shown in fig. 4(a).i–vi. The location of the asperity is indicated by a red arrow in fig. 4(a).v. From the height traces $h(t)$ corresponding to a contact event, as shown for one example in fig. 4(b), we estimate the lifetime of the air film preceding contact with an asperity Δt by taking the difference between the first-passage time and the time of contact, indicated by the vertical bars in fig. 4(b); ultimately, contact occurs at height h_n, as indicated in the figure. Contact nucleates on asperities sporadically, consistent with the broadly distributed $\Delta t(h)$ plotted in fig. 4.

If the film of air is thin enough it will rupture, leading to multiple liquid bridges that bind the drop to the surface

[2] `http://youtu.be/Nf810Ompreg`.

[3] Video accessible at `http://youtu.be/XXmOoHEiRCM`.

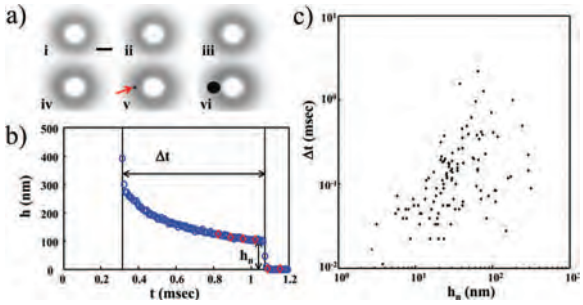

Fig. 4: (Color online) Stability of the thin film of air confined between an impacting drop and a hydrophilic glass surface. (a) A time series of images recorded using the TIR technique. Each image is separated by 66 μs, and the scale-bar in i represents 250 microns. Contact initiates suddenly at a location highlighted by the red arrow in frame v at $h = 100$ nm. The asperity is smaller than the lateral resolution of our optics, and thus does not appear in the images preceding contact. At the moment of contact initiation, the global minimum thickness of the air film $h_m \sim 96$ nm, significantly lower than the height at the point of contact. (b) $h(t)$ for the time series shown in (a); red diamonds corresponded to each snapshot. The air slowly drains and the thickness of the film decreases to a minimal thickness $h_n = 100$ nm over a time Δt. Δt is measured from the first passage time of the liquid over the point of interest until the initiation of contact, at $t = 1.08$ ms. (c) $\Delta t(h_n)$ for 44 impact experiments and 111 contacts that initiate beneath an impacting water-glycerol droplet on a smooth glass surface; in each experiment, $V < V_c$.

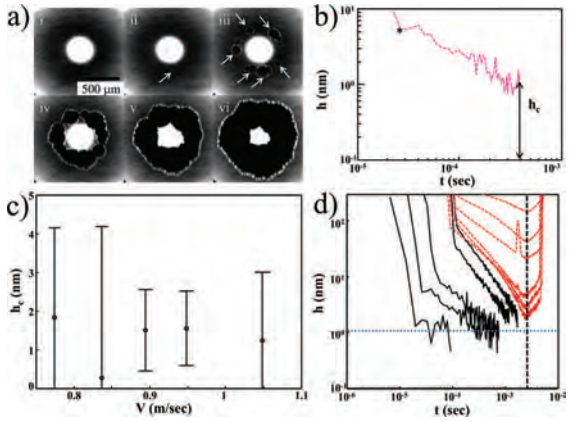

Fig. 5: (Color online) Stability and breakdown of the thin film of air. (a) A sequence of typical images for a $R = 800\,\mu$m drop impacting at $V = 0.89$ m/s. In order to highlight the dynamics occurring less than 10 nm above the surface, contrast is enhanced and white corresponds to all heights greater than 17.5 nm. Contact is depicted by bright rings and initiates at discrete points in ii; the contacts subsequently grow in iii, and merge into a closed ring in iv. The contacts continue to grow outward and inward from the ring in v, vi. Subsequent images are separated by 27 μs. (b) $h(t)$ at a point where contact initiated for $R = 800\,\mu$m and $V = 0.94$ m/s. The initial film thickness, indicated by the asterisk (*), is 5.5 nm, and the film ruptures at $h_c = 1$ nm. (c) Rupture height, h_c, as a function of V for $R = 800\,\mu$m. For $V < V_c = 0.75$ m/s the film never ruptures and the drops bounce away from the surface. (d) $h(t)$ traces for $V < V_c$ (red) and $V > V_c$ (black). The typical reversal time, t^*, and h_c are indicated by the vertical dashed line, and the horizontal dotted line, respectively.

(fig. 5(a)) and prevent bouncing. Thus, at large impact velocities, when the thickness of the air film is small, the film may drain to a nanometric critical thickness h_c, and subsequently rupture, as shown in fig. 5(b). h_c does not depend on impact velocity, as shown in fig. 5(c), indicating that the mechanism for air film rupture is dominated by surface forces. Our nanometric values of h_c measured above mica surfaces are significantly lower than the scales we measured for impact on glass surfaces, which may exceed 400 nm [31]; we attribute this discrepancy to geometric defects on the glass surface that nucleate liquid-solid contact and prevent rebound. Indeed, for hydrophilic surfaces, any single asperity will nucleate a liquid bridge that will rapidly spread and destroy the entire thin film of air, as shown in fig. 4(c). While the absence of asperities is readily achieved with freshly cleaved mica, it does not consistently occur for glass. Although the root-mean-squared (RMS) roughness value is typically of the order of a single nanometer for such glass surfaces [18], even carefully cleaned glass surfaces will have sparse asperities and defects; although they may be statistically insignificant, these asperities can exceed the air film thickness, and dominate the dynamics in a majority of impact events on glass surfaces. Nevertheless, on rare occasions, we observe rebound from regular glass slides and silicon wafers, as shown in the supplementary video[4]. Thus, on all but smooth, defect-free surfaces, drop impact is characterized by the nucleation of capillary bridges at asperities. For a smooth surface the transition from bouncing to spreading occurs only if the thin film of air can drain to h_c and rupture. This is demonstrated by the black line in fig. 5(d). However, if the thin film of air does not reach the critical thickness before the half-period of a capillary-induced oscillation, the liquid drop will completely rebound, as demonstrated by the blue line in fig. 5(d).

It has long been known that solid particles immersed in a viscous fluid can bounce off surfaces without ever making contact [32] due to a combination of effects associated with elastic deformation of the surface and lubrication-induced forces in the fluid. Here we have shown that the deformation of the drop and the thin film of air that separates it from a macroscopic and smooth hydrophilic surface can also lead to drop bouncing, adding a new facet to the role of the thin air film in droplet impact: not only can it affect splashing, but in fact under appropriate conditions it can completely reverse the motion of the drop and cause it to bounce, albeit gently, owing to viscous dissipation in the air cushion between the drop and the substrate. These effects require that the surface be smooth over the entire drop-spreading area; this is likely to be the case for specialized surfaces such as mica, but can also occur for micro fabrication processes on a variety of surfaces, where

[4]Video accessible at `http://youtu.be/Jd54tMI7xFw`.

very small drops are deposited. The strikingly small values of $h_c \sim 1\,\mathrm{nm}$ are far less than those predicted for the onset of instability in thin viscous films [25]; this strident disagreement between our measurements and the theoretical prediction suggests that the thin film of air is anomalously stable, and demands further inquiry.

However, on most hydrophilic surfaces where wetting dynamics are dominated by the presence of discrete defects, bouncing is the anomaly rather than the rule. Therefore, new methods for surface characterization are required for predicting and controlling droplet impact on smooth hydrophilic surfaces.

* * *

This work was supported by ISF grant No. 1415/12 and Harvard MRSEC (DMR-0820484). We thank Rivka Maoz and Jacob Sagiv for help in surface characterization and Elisha Moses, Aaron Mowitz, and Irit Goldian for useful discussions. We acknowledge support from the NSF GRFP (JMK) and the MacArthur Foundation (LM).

REFERENCES

[1] Yarin A. L., *Annu. Rev. Fluid Mech.*, **38** (2006) 159.
[2] Xu L., Zhang W. W. and Nagel S. R., *Phys. Rev. Lett.*, **94** (2005) 184505.
[3] Xu L., *Phys. Rev. E*, **75** (2007) 056316.
[4] Rein M. and Delplanque J. P., *Acta Mech.*, **201** (2008) 105.
[5] Latka A., Strandburg-Peshkin A., Driscoll M. M., Stevens C. S. and Nagel, S. R., *Phys. Rev. Lett.*, **109** (2012) 054501.
[6] Leidenfrost J. G., *Int. J. Heat Mass Transfer*, **9** (1756) 1153.
[7] Richard D. and Quéré D., *Europhys Lett.*, **50** (2000) 769.
[8] Onda T., Shibuichi S., Satoh N. and Tsujii K., *Langmuir*, **12** (1996) 2125.
[9] Shibuichi S., Onda T., Satoh N. and Tsujii K., *J. Phys. Chem.*, **100** (1996) 19512.
[10] Bird J. C., Dhiman R., Kwon H. M. and Varanasi K. K., *Nature*, **503** (2013) 385.
[11] Couder Y., Fort E., Gautier C. H. and Boudaoud A., *Phys. Rev. Lett.*, **94** (2005) 177801.
[12] Kolinski J. M., Rubinstein S. M., Mandre S., Brenner M. P., Weitz D. A. and Mahadevan L., *Phys. Rev. Lett.*, **108** (2012) 074503.
[13] Okumura K., Chevy F., Richard D., Quéré D. and Clanet C., *Europhys Lett.*, **62** (2003) 237.
[14] Driscoll M. M. and Nagel S. R., *Phys. Rev. Lett.*, **107** (2011) 154502.
[15] Driscoll M. M., Stevens C. S. and Nagel S. R., *Phys. Rev. E*, **82** (2010) 036302.
[16] Xu L., Barcos L. and Nagel S. R., *Phys. Rev. E*, **76** (2007) 066311.
[17] van der Veen R. C. A., Tran T., Lohse D. and Sun C., *Phys. Rev. E*, **85** (2012) 026315.
[18] Mandre S. and Brenner M. P., *J. Fluid Mech.*, **690** (2012) 148.
[19] Mandre S., Mani M. and Brenner M. P., *Phys. Rev. Lett.*, **102** (2009) 134502.
[20] Mani M., Mandre S. and Brenner M. P., *J. Fluid Mech.*, **647** (2010) 163.
[21] Thoroddsen S. T., Etoh T. G. and Takehara K., *J. Fluid Mech.*, **478** (2003) 125.
[22] Thoroddsen S. T., Etoh T. G., Takehara K., Ootsuka N. and Hatsuki Y., *J. Fluid Mech.*, **545** (2005) 203.
[23] Kolinski J. M., Mahadevan L. and Rubinstein S. M., *Phys. Rev. Lett.*, **112** (2014) 134501.
[24] Rioboo R., Marengo M. and Tropea C., *Exp. Fluids*, **33** (2002) 112.
[25] Brochard-Wyart F. and Daillant J., *Can. J. Phys.*, **68** (1990) 1084.
[26] Rayleigh L., *Proc. R. Soc.*, **29** (1879) 71.
[27] Richard D., Clanet C. and Quéré D., *Nature*, **417** (2002) 811.
[28] Truesdell R., Mammoli A., Vorobieff P., van Swol F. and Brinker C. J., *Phys. Rev. Lett.*, **97** (2006) 044504.
[29] Choi C. H. and Kim C. J., *Phys. Rev. Lett.*, **96** (2006) 066001.
[30] Taylor G. I., *Proc. R. Soc. London, Ser. A*, **259** (1960) 1.
[31] de Ruiter J., Oh J. M., van den Ende D. and Mugele F., *Phys. Rev. Lett.*, **108** (2012) 074505.
[32] Davis R. H., Serayssol J. M. and Hinch E., *J. Fluid Mech.*, **163** (1986) 479.